Radiance and Polarization of Multiple Scattered Light from Haze and Clouds

George W. Kattawar and Gilbert N. Plass

The radiance and polarization of multiple scattered light is calculated from the Stokes' vectors by a Monte Carlo method. The exact scattering matrix for a typical haze and for a cloud whose spherical drops have an average radius of 12 μ is calculated from the Mie theory. The Stokes' vector is transformed in a collision by this scattering matrix and the rotation matrix. The two angles that define the photon direction after scattering are chosen by a random process that correctly simulates the actual distribution functions for both angles. The Monte Carlo results for Rayleigh scattering compare favorably with well known tabulated results. Curves are given of the reflected and transmitted radiances and polarizations for both the haze and cloud models and for several solar angles, optical thicknesses, and surface albedos. The dependence on these various parameters is discussed.

I. Introduction

The transmission and reflection of light by an atmosphere composed of any arbitrary mixture of aerosols and Rayleigh scattering centers can be treated by a Monte Carlo method.[1,2] The exact scattering function calculated from the Mie theory,[3] including the typical strong forward scattering maximum, is used in this method. The photon is followed through multiple scatterings as long as it makes any appreciable contribution to the intensity.

Our work has previously used the linear theory, whereas a complete description of the scattering process requires the use of the Stokes' vectors.[4] Chandrasekhar[4] has shown that the intensity calculated from Rayleigh's phase function by a linear theory generally differs from the correct intensity obtained by the use of Stokes' vectors. He showed that differences of the order of 10% occur between values of the total intensity calculated by these two methods for some values of the parameters. Although it might be anticipated that these differences might be less for a Mie phase function, no data have been available that might be used to check this point.

In this paper, our Monte Carlo work is extended to include an exact description of the scattering process that uses a scattering matrix and the Stokes' vectors. The results are checked for the case of Rayleigh scattering against the tabulations of Coulson *et al.*[5] The intensity and polarization of the reflected and transmitted light is calculated for a haze and for nimbostratus clouds. Several thicknesses and angles of incidence are considered.

The authors are with the Southwest Center for Advanced Studies, P. O. Box 30365, Dallas, Texas 75230.

Received 25 September 1967.

II. Method of Calculation

Our previous Monte Carlo code,[1] which calculates radiances due to photons that have undergone multiple scattering, has been extended to include the four component Stokes' vector. Of the possible choices for the Stokes' components, the set I, Q, U, and V seems to be the most advantageous in Monte Carlo calculations. The total intensity I and the quantity V are both invariant under a rotation of the reference axes. Thus, the flux can be estimated at each collision without rotation of the axes. The rotation matrix itself is also simpler in this representation.

The Stokes' vector after a scattering event (unprimed variables) is obtained from the Stokes' vector before the scattering (primed variables) from the transformation:

$$\begin{pmatrix} I \\ Q \\ U \\ V \end{pmatrix} = \begin{pmatrix} 1 & 0 & 0 & 0 \\ 0 & \cos 2i_2 & -\sin 2i_2 & 0 \\ 0 & \sin 2i_2 & \cos 2i_2 & 0 \\ 0 & 0 & 0 & 1 \end{pmatrix} \times \begin{pmatrix} \tfrac{1}{2}(M_2 + M_1) & \tfrac{1}{2}(M_2 - M_1) & 0 & 0 \\ \tfrac{1}{2}(M_2 - M_1) & \tfrac{1}{2}(M_2 + M_1) & 0 & 0 \\ 0 & 0 & S_{21} & -D_{21} \\ 0 & 0 & D_{21} & S_{21} \end{pmatrix} \times \begin{pmatrix} 1 & 0 & 0 & 0 \\ 0 & \cos 2i_1 & -\sin 2i_1 & 0 \\ 0 & \sin 2i_1 & \cos 2i_1 & 0 \\ 0 & 0 & 0 & 1 \end{pmatrix} \begin{pmatrix} I' \\ Q' \\ U' \\ V' \end{pmatrix}. \quad (1)$$

The four quantities in the scattering matrix M_1, M_2, S_{21}, and D_{21} are identical with the definitions of Van de Hulst (Ref. 6, see p. 44). The angles i_1 and i_2 in the rotation

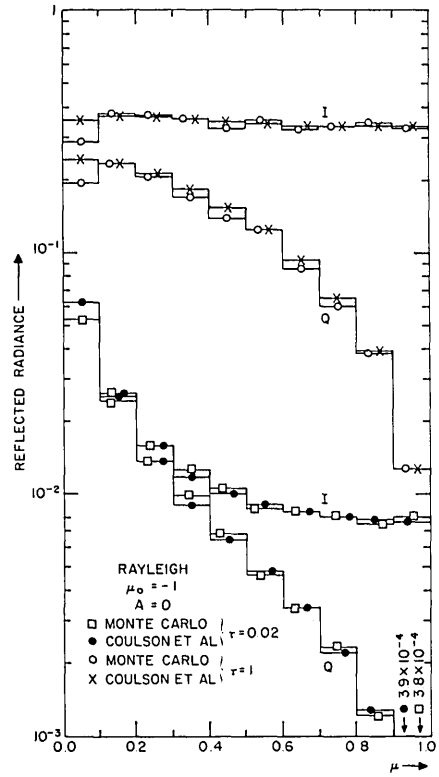

Fig. 1. Reflected radiance as a function of the cosine of the zenith angle (μ) for Rayleigh scattering. The Stokes' vectors I and Q are shown for both $\tau = 0.02$ and 1. The results of the Monte Carlo calculation are compared with those of Coulson *et al.*[5] averaged over the same μ intervals. For all these curves, the cosine of the incident angle (μ_0) is -1 and the surface albedo $A = 0$.

matrix are used as defined by Chandrasekhar (Ref. 4, p. 39 and Fig. 8).

In the Monte Carlo method, the scattering angle θ is selected by a random process from the cumulative distribution of the scattering function $\frac{1}{2}(M_1 + M_2)$; similarly the angle i_1 is chosen from a uniform distribution between 0 and 2π. These distributions are a first approximation to the correct distributions for θ and i_1. The calculation allows for the difference between the actual distribution and the approximate one by correcting the components of the Stokes' vector after collision by a method described below. It should be emphasized that the procedure would yield the correct result for any initial distribution function for θ and i_1, but the statistical fluctuations are less if the initial distribution functions are reasonably close to the actual ones. Once the angles θ and i_1 have been selected, the angle i_2 is computed from the equations of spherical trigonometry. It should be noted that it is not necessary to sample θ and i_1 from a bivariate distribution,[7] but instead a biased distribution may be used.

Any Monte Carlo calculation may be reduced to the evaluation of a multidimensional integral, i.e., the computation of the expectation value E of some function $f(\eta_1, \eta_2, \ldots, \eta_m)$ of the random variables $\eta_1, \eta_2, \ldots, \eta_m$ with probability density functions $p_1(\alpha), p_2(\alpha), \ldots, p_m(\alpha)$. If at each stage of construction of the path we play for the variable ϵ_k with the probability density function $p_k^*(\alpha)$ instead of η_k, we obtain a different path and the averaged function $f^*(\epsilon_1, \epsilon_2, \ldots, \epsilon_m)$ becomes

$$f^*(\epsilon_1,\ldots,\epsilon_m) = f(\epsilon_1,\ldots,\epsilon_m) \times [p_1(\epsilon_1)\ldots p_m(\epsilon_m)]/[p_1^*(\epsilon_1)\ldots p_m^*(\epsilon_m)]. \quad (2)$$

The same expectation value is obtained in either case, since

$$\begin{aligned} Ef^*(\epsilon_1,\ldots,\epsilon_m) &= \int_{x_1,\ldots,x_m} f(x_1,\ldots,x_m)\{[p_1(x_1)\ldots p_m(x_m)]/ \\ &\quad [p_1^*(x_1)\ldots p_m^*(x_m)]\}\,[p_1^*(x_1)\ldots p_m^*(x_m)]dx_1\ldots dx_m \\ &= \int_{x_1,\ldots x} f(x_1,\ldots,x_m)[p_1(x_1)\ldots p_m(x_m)]dx_1\ldots dx_m \\ &= Ef(\eta_1,\ldots,\eta_m). \end{aligned} \quad (3)$$

Although f^* and f have the same expectation values, their variances are different in general.

In order to understand the application of the above method to our problem, consider the intensity I after a scattering event, but before the final rotation through the angle i_2. From Eq. (1) it is found that

$$I(\Theta,i_1) = \tfrac{1}{2}I'(M_1 + M_2) + \tfrac{1}{2}(M_2 - M_1) \times (Q'\cos 2i_1 - U'\sin 2i_1), \quad (4)$$

with similar relations for Q, U, and V. The random variable Θ is sampled from the distribution $\frac{1}{2}(M_1 + M_2)$ and i_1 is chosen uniformly between 0 and 2π. The

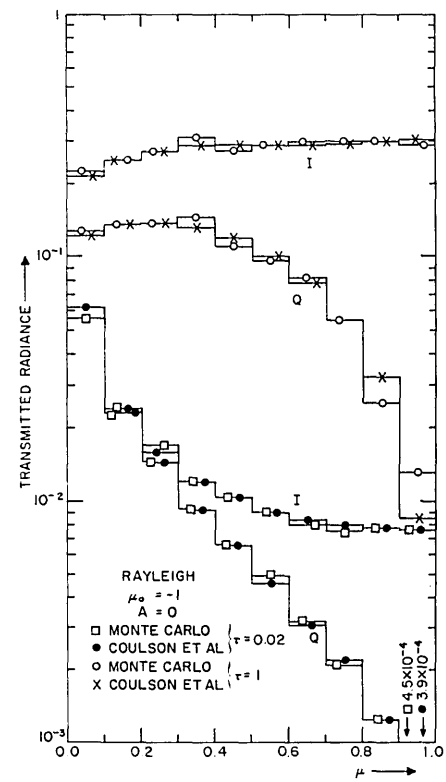

Fig. 2. Transmitted radiance as a function of μ for Rayleigh scattering. See caption for Fig. 1.

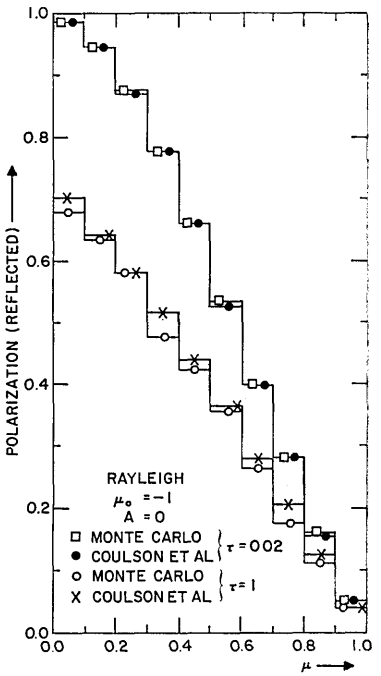

Fig. 3. Polarization of the reflected radiation as a function of μ for Rayleigh scattering. See caption for Fig. 1.

Stokes' vector **I** is then divided by this distribution function. The expectation value of the resulting vector is the same as though it had been sampled from the correct distribution in both Θ and i_1. The angle Θ is sampled from the function $\frac{1}{2}(M_1 + M_2)$ in order to improve the statistics of the calculation, particularly when there is strong forward scattering.

This method was tested by comparing the values tabulated by Coulson *et al.*[5] for Rayleigh scattering with the results of the Monte Carlo method. The intensities are shown in Figs. 1 and 2 for optical thicknesses $\tau = 0.02$ and 1. Both the total intensity I and the difference of the two components of the intensity $Q = I_r - I_l$ are shown. The agreement is excellent when consideration is given to the inevitable statistical fluctuations in the Monte Carlo results. For $\tau = 0.02$ and 1, the number of photon histories calculated was 10,000 and 5000, respectively; these represented calculation times of 15 mm and 50 min, respectively, on the IBM model 360–50 electronic computer. A comparison of the polarizations calculated for Rayleigh scattering (using the definition of polarization given by Coulson *et al.*[5]) is shown in Figs. 3 and 4. For both τ values, the agreement is excellent. The results of Coulson *et al.*[5] in all these figures are numerically averaged before they are plotted over the same μ interval as was used in the Monte Carlo calculation.

III. Scattering Function

Two different models of clouds and hazes are considered in this paper. The first is the continental haze model (haze *C*) proposed by Deirmendjian.[3] The particle concentration is zero for radii less than 0.03 μ; is 10^3 cm^{-3} μ^{-1} for radii between 0.03 μ and 0.1 μ; is $0.1r^{-4}$ cm^{-3} μ^{-1} for radii greater than 0.1 μ. The second model (nimbostratus) represents clouds with moderately large water drops. The particle concentration $n(r)$ is assumed to be

$$n(r) = 0.00108\, r^6 \exp(-0.5\, r). \tag{5}$$

The maximum particle concentration occurs when $r = 12\,\mu$.

The scattering matrix was calculated for each of these models from the Mie theory by a method previously described.[3] The elements of the matrix were averaged over the particle size distribution by a very accurate integration routine. A wavelength of 0.7 μ for the incident light and a real index of refraction of 1.33 for the water droplets was assumed for this calculation. The scattering matrix was calculated at 0.25° intervals in the forward direction near the strong forward scattering maximum and at 2° intervals in the backward direction where the elements undergo oscillations. At the remaining angles the elements for the nimbostratus model were calculated at 2° intervals and those of the haze *C* model at 5° intervals.

The matrix elements calculated in this manner were used in the Monte Carlo calculation as described in Sec. II. The results for the elements of the scattering matrix are shown in Figs. 5 and 6. The elements for the nimbostratus model do not vary as smoothly as those for the more moderate radii of the haze *C* model. Because of the many rapid fluctuations of the elements S_{21} and D_{21} for the nimbostratus model, it was not possible to plot them when their values were less than 7×10^{-4}.

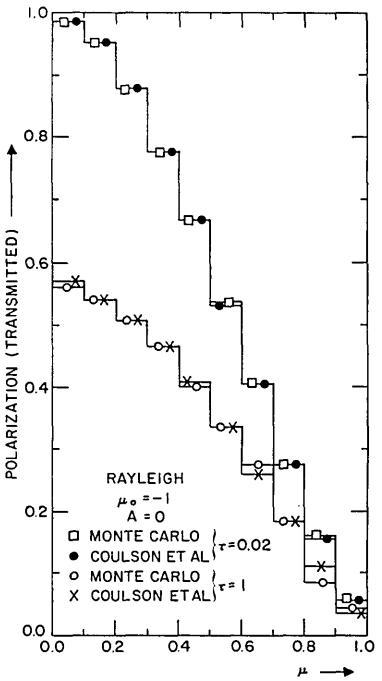

Fig. 4. Polarization of the transmitted radiation as a function of μ for Rayleigh scattering. See caption for Fig. 1.

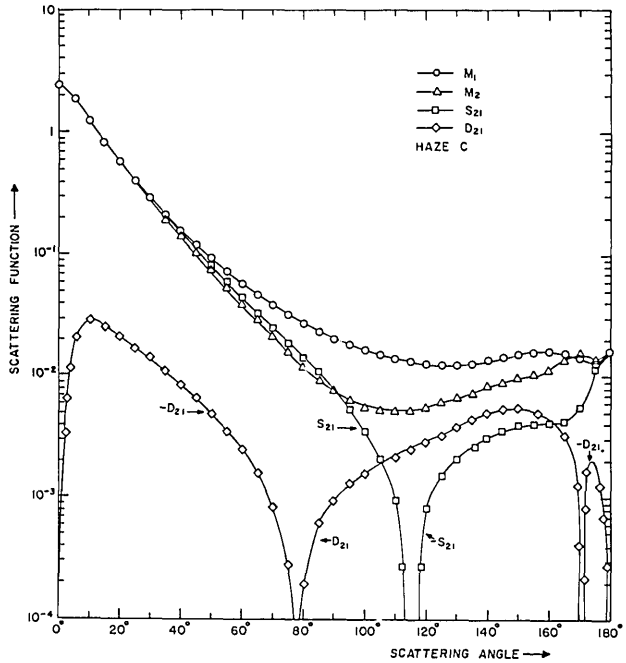

Fig. 5. Four elements (M_1, M_2, S_{21}, D_{21}) of the scattering matrix as a function of the scattering angle Θ for the haze C model.

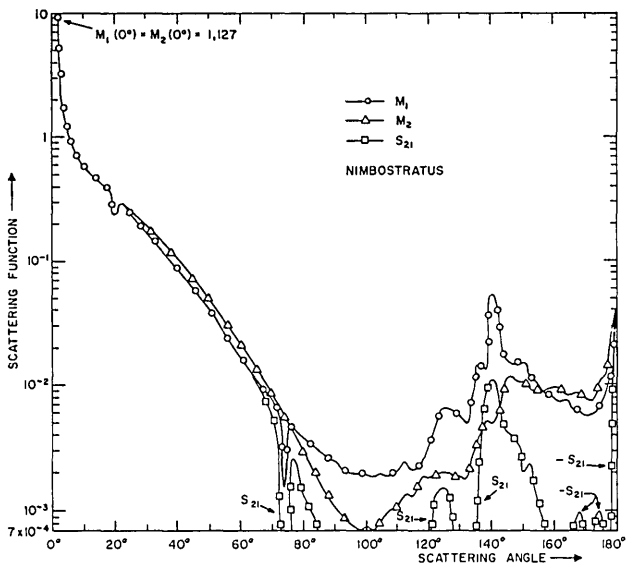

Fig. 6. Four elements (M_1, M_2, S_{21}, D_{21}) of the scattering matrix as a function of the scattering angle Θ for the nimbostratus model.

All calculations reported here assume a single scattering albedo ω_0 of unity and reflection from a Lambert's surface as representative of the planetary surface. The incident flux is normalized to unity (instead of the value π sometimes chosen).

IV. Reflected Radiance

The reflected radiance was calculated from the scattering matrix for two optical thicknesses ($\tau = 0.1$ and 1), two angles of incidence (cosine of incident angle $\mu_0 = -1$ and -0.1), and for the two models (haze C and nimbostratus). The results for a surface albedo $A = 0$ and 0.8 and for $\mu_0 = -1$ are shown in Fig. 7. For comparison purposes, the reflected radiances calculated from the linear theory using a scalar scattering function are also shown. In most cases, there is very little difference between the results calculated from the linear and from the Stokes' vector methods. Where there are differences, the values for one case seem to be as often

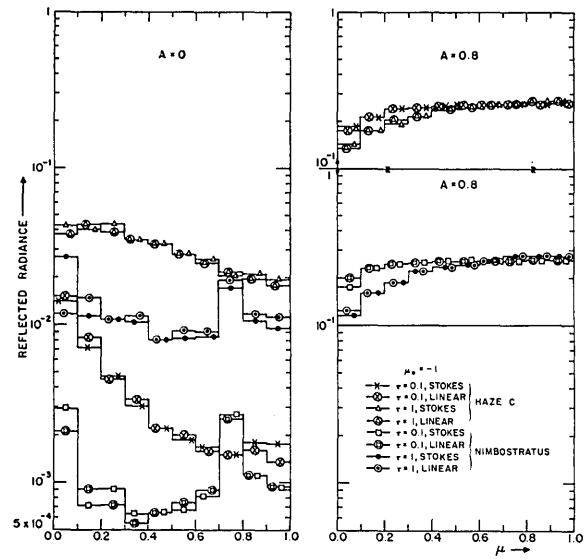

Fig. 7. Reflected radiance as a function of the cosine of the zenith angle (μ) for $A = 0$ and $A = 0.8$ and $\mu_0 = -1$. Curves are shown for $\tau = 0.1$ and 1 and for the haze C and nimbostratus models. The results obtained from the linear theory and from Stokes' vectors are compared.

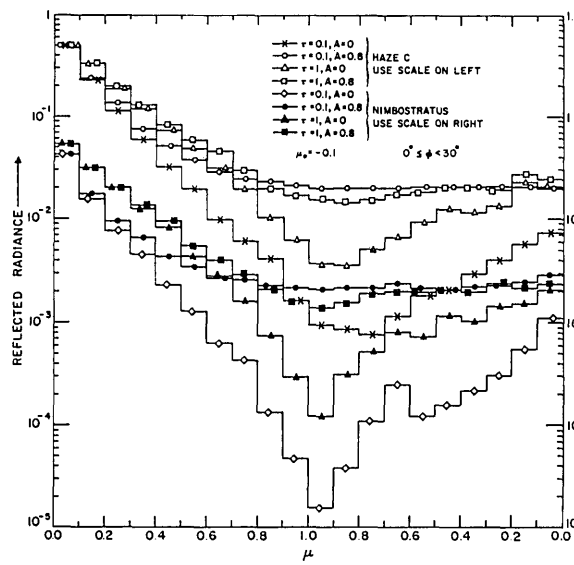

Fig. 8. Reflected radiance as a function of μ for $\mu_0 = -0.1$ and $A = 0$ and 0.8. The results have been averaged over the azimuth angle ϕ measured from the incident plane for 0° to 30° on both sides of this plane. On all curves the solar horizon is on the left-hand side of the figure and the antisolar horizon on the right-hand side.

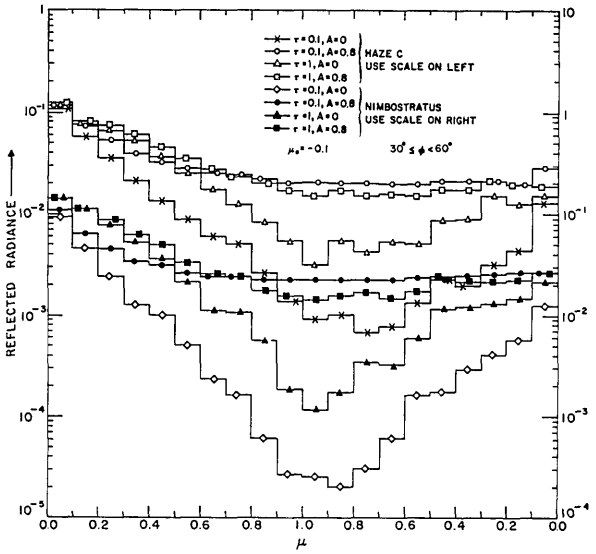

Fig. 9. Reflected radiance as a function of μ. Same as Fig. 8 except that the results have been averaged over ϕ from 30° to 60° on both sides of the incident plane.

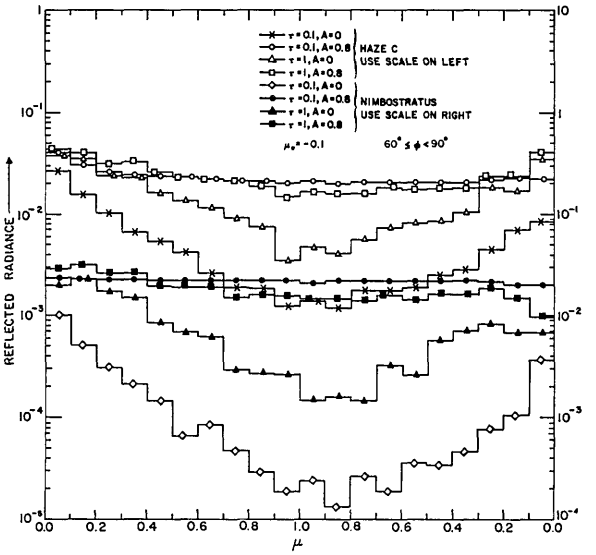

Fig. 10. Reflected radiance as a function of μ. Same as Fig. 8 except that the results have been averaged over ϕ from 60° to 90° on both sides of the incident plane.

above as below those for the other case. Thus, many of these differences are undoubtedly due to statistical fluctuations in the Monte Carlo results. When $\tau = 0.1$, 10,000 photon histories were processed and when $\tau = 1$, 7000, and 5000 photon histories were processed for $\mu_0 = -1$ and -0.1, respectively.

These results must be interpreted in terms of the elements of the scattering matrix. Many of the wiggles in the radiance curves that appear at first sight to be statistical fluctuations are real and result from variations in the scattering matrix. For example, the increased radiance values between $\mu = 0.7$ and 0.8 for the nimbostratus model are the result of the sharp maximum in the M_1 values at the corresponding angles and are not fluctuations.

The reflected radiance when $\mu_0 = -0.1$ is shown in Figs. 8–10 as a function of the cosine of the nadir angle (μ). The solar horizon is always on the left-hand side of these figures and the antisolar horizon on the right-hand side. The values shown in Fig. 8 have been averaged over the azimuth angle ϕ measured from the incident plane from 0° to 30° on both sides of this plane. The values shown in Fig. 9 have been averaged over ϕ from 30° to 60° on both sides of the incident plane. Similarly, Fig. 10 gives the values averaged over ϕ from 60° to 90°. The variation of the radiance with μ is usually much more pronounced for photons whose ϕ value is in the first of these three ranges compared with those in the last of these ranges.

There is a pronounced increase in the radiance near the solar horizons when ϕ is near 0° and relatively little increase when ϕ is nearer 90°. The increase in the first case is caused by the numerous small angle scattering events specified by our scattering matrix, whereas in the second case, the scattering angles must be nearer 90° and thus a much smaller number of photons are scattered into these angles. Note that in these figures the scale on the left should be used for the haze C model and the scale on the right for the nimbostratus model. The curves for the nimbostratus model are almost always below the corresponding curves for the haze C model when $\phi > 30°$, since the corresponding scattering angles are fairly large and the probability of scattering into these larger angles is considerably less for the nimbostratus model than for the haze C model.

V. Transmitted Radiance

The transmitted radiance for $\mu_0 = -1$ is shown in Fig. 11. Here once again we have compared the results of the calculation from the linear theory with a scalar scattering function and the calculation with the Stokes' vectors. Once more the differences between the two results seem quite small. When they do appear, they

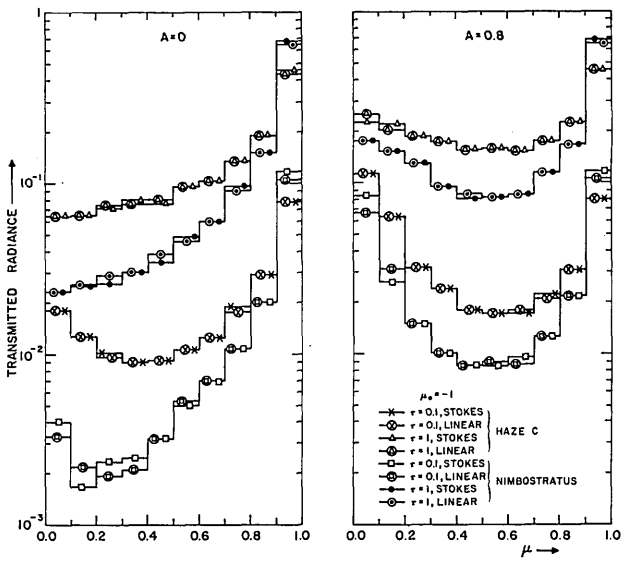

Fig. 11. Transmitted radiance as a function of μ. See caption for Fig. 7.

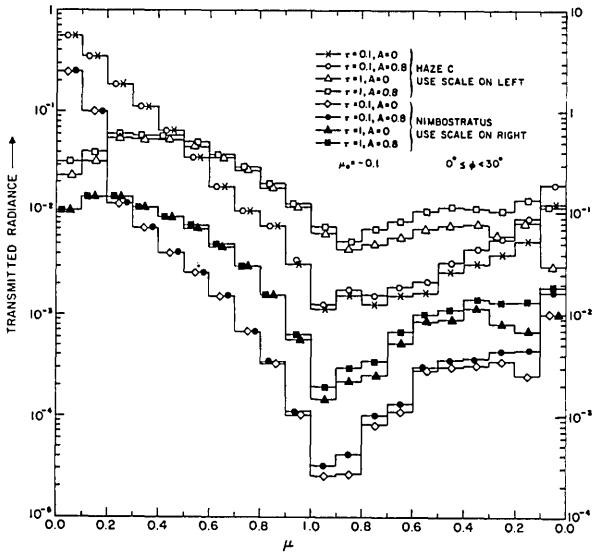

Fig. 12. Transmitted radiance as a function of μ. See caption for Fig. 8.

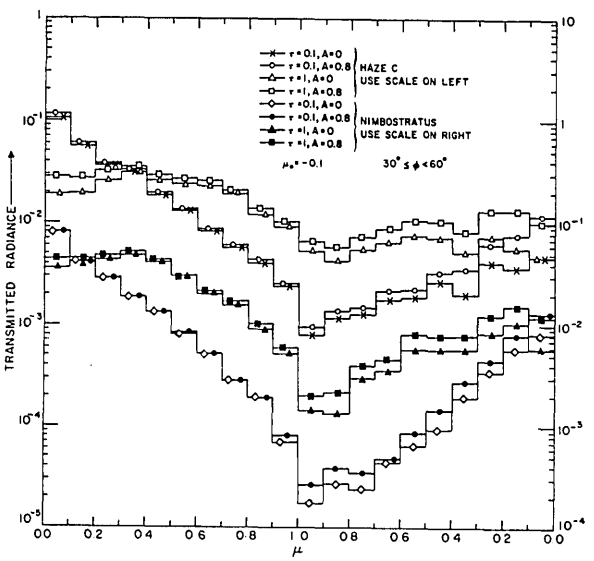

Fig. 13. Transmitted radiance as a function of μ. See caption for Fig. 9.

do not show any consistent trend and are probably mostly due to statistical fluctuations. The differences are much smaller between the two methods of calculation when a Mie scattering matrix with strong forward scattering is used than when the Rayleigh matrix is assumed. This is because in the Rayleigh case the difference between the two polarized components of the intensity reaches a maximum at a scattering angle of 90°, since one component of the intensity approaches zero at 90°. In the present models, there is no such large difference between the two components at any scattering angle and on the average they are much closer to each other. Thus, it seems established that the total intensity can be obtained with reasonable accuracy for a Mie particle from the linear theory, provided that the differences between the two components is not too large on the average. Of course, the complete theory with the Stokes' vectors should be used if polarization information is desired or if there are an appreciable number of Rayleigh scattering centers in the atmosphere.

The transmitted radiance when $\mu_0 = -0.1$ is given in Figs. 12–14. In these figures, use the scale on the left for the haze C model and the scale on the right for the nimbostratus model. When the transmitted photon is near the incident plane, the maximum radiance value occurs on the solar horizon when $\tau = 0.1$. This is caused by the numerous small angle scattering events. When $\tau = 1$, the maximum occurs above the solar horizon. The maximum is much less prominent at other ϕ angles. At angles away from the direction of the incident beam, the radiance is less in most cases for the nimbostratus model than for the haze C model. This is because the probability for scattering through a given angle is greater for the haze C model than for the nimbostratus model for all scattering angles except those near 0° and those near the sharp peak in M_1 near $\cos\theta = -0.8$.

VI. Polarization of Reflected Light

The polarization of the reflected light is calculated as part of our Monte Carlo code. There are several definitions of polarization. In this section we use the Rubenson definition of the degree of polarization P as

$$P = Q/I = (I_r - I_l)/(I_r + I_l). \tag{6}$$

The components U and V are small compared with I and Q in almost all cases calculated here, so that this polarization gives results very close to those obtained from the definition involving U and V. In addition, the sign of the Rubenson degree of polarization defines the orientation of the plane of polarization of the scattered light. When it is positive, the plane of polariza-

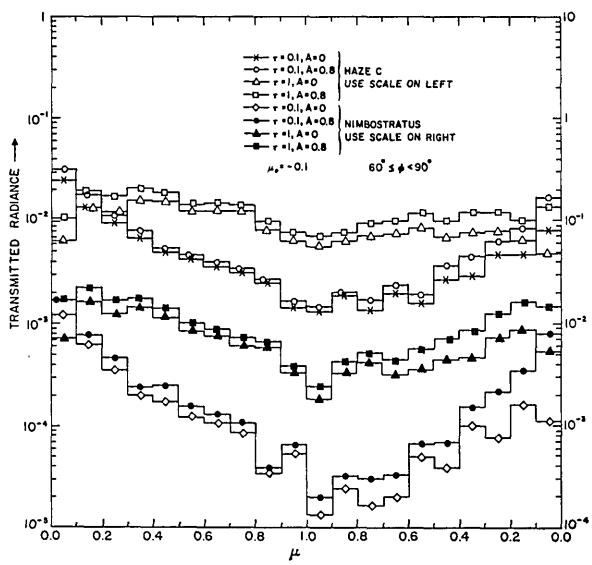

Fig. 14. Transmitted radiance as a function of μ. See caption for Fig. 10.

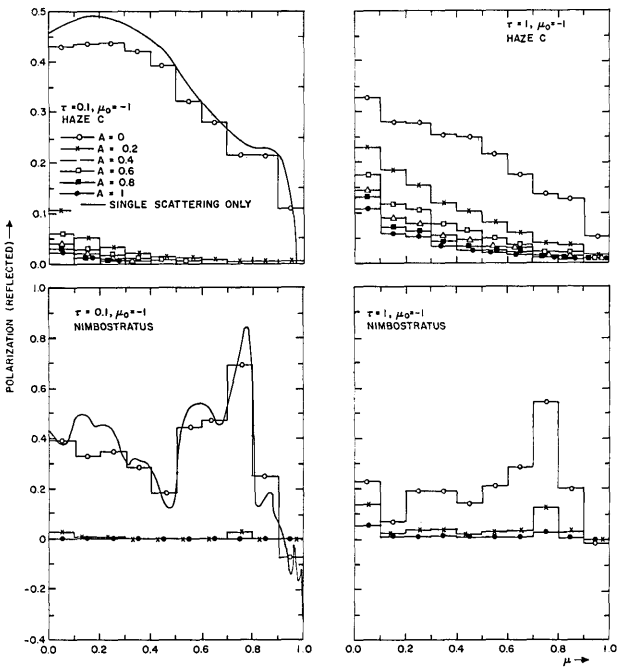

Fig. 15. Polarization of reflected radiation as a function of μ. Curves are shown for $\tau = 0.1$ and 1, $\mu_0 = -1$, haze C and nimbostratus models, and $A = 0$, 0.2, 0.4, 0.6, 0.8, and 1. The continuous solid curve is the polarization calculated from the scattering matrix for single scattering events only.

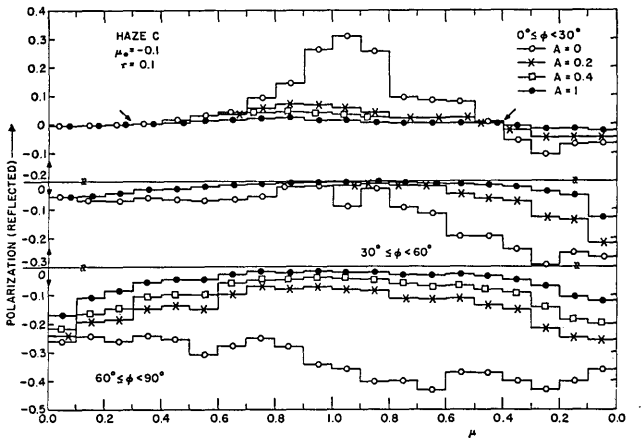

Fig. 16. Polarization of reflected radiation as a function of μ. Curves are shown for the haze C model, $\mu_0 = -0.1$, $\tau = 0.1$, and $A = 0$, 0.2, 0.4, and 1. The results have been averaged over ϕ from 0° to 30° on both sides of the incident plane for the top set of curves; from 30° to 60° for the middle set of curves; and from 60° to 90° for the bottom set of curves.

tion of the scattered light is perpendicular to the scattering plane.

The polarization when $\mu_0 = -1$ is shown in Fig. 15. Values are given for a number of surface albedos A. The curves for $\tau = 0.1$ show for comparison purposes the polarization calculated from single scattering only. It is seen that the polarization calculated from the Monte Carlo method for $A = 0$ closely follows the average value of the single scattering curve, except near the horizon where multiple scattering reduces the polarization values. Particularly for the nimbostratus model, the Monte Carlo results by themselves would appear rather strange and as though they had large fluctuations. However, the single scattering curve shows that they faithfully reproduce the many sharp peaks and valleys in this curve.

When $\tau = 0.1$, the polarization is large only when the surface albedo is near zero. When $A = 0.2$, the polarization is nearly zero except very close to the horizon. This of course is due to the strong unpolarized flux of radiation that is reflected from the surface and can easily penetrate a cloud with the relatively small τ value of 0.1. When $\tau = 1$, it is interesting to see how the polarization values for $A = 0$ are reduced from those for $\tau = 0.1$ by multiple scattering. However, when some radiation is reflected from the surface, the polarization is larger in every case for $\tau = 1$ than for

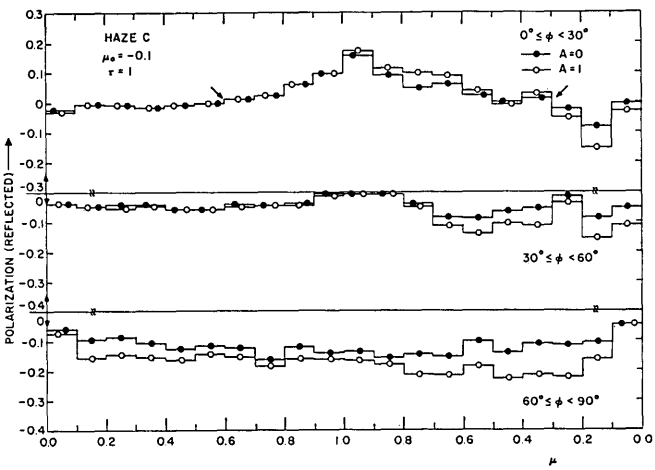

Fig. 17. Polarization of reflected radiation as a function of μ. Same as Fig. 16 except $\tau = 1$.

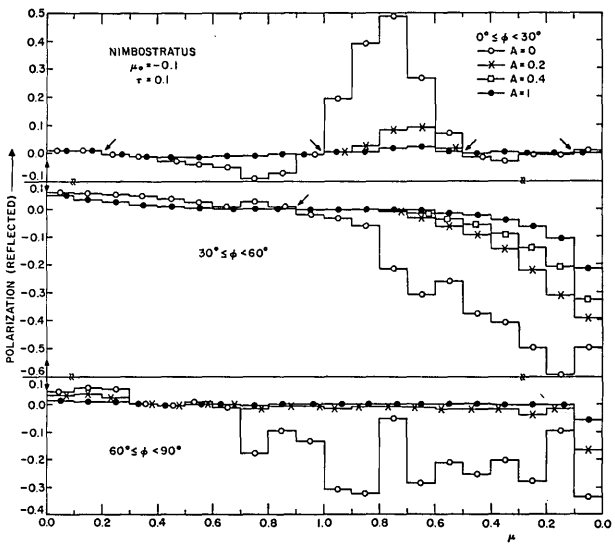

Fig. 18. Polarization of reflected radiation as a function of μ. Same as Fig. 16 except for nimbostratus model.

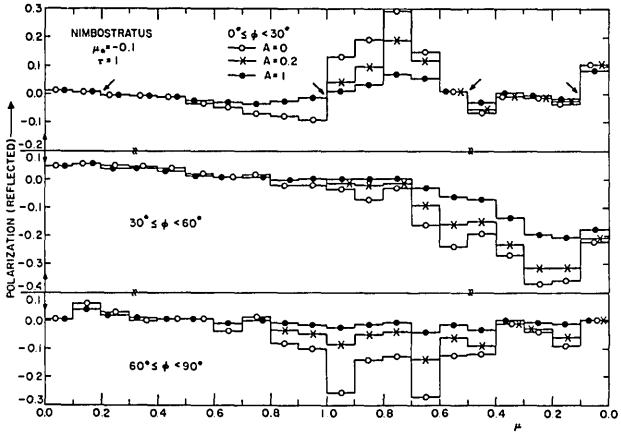

Fig. 19. Polarization of reflected radiation as a function of μ. Same as Fig. 17 except for nimbostratus model.

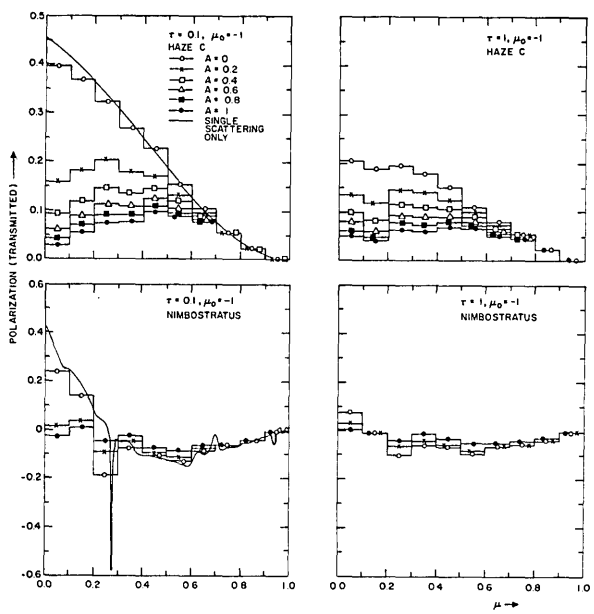

Fig. 20. Polarization of transmitted radiation as a function of μ. Curves are shown for the haze C and nimbostratus models, $\tau = 0.1$ and 1, $\mu_0 = -1$, and $A = 0, 0.2, 0.4, 0.6, 0.8$, and 1. The continuous solid curve is the polarization calculated from the scattering matrix for single scattering only.

$\tau = 0.1$. This is because the radiation that is unpolarized after reflection from a Lambert's surface undergoes on the average one or more collisions before leaving the upper surface of the cloud when $\tau = 1$ and becomes partially polarized by these collisions. The nimbostratus polarization still has a strong maximum for μ between 0.7 and 0.8 corresponding to the large difference between the elements M_1 and M_2 of the scattering matrix. For a given nonzero surface albedo A, the polarization for the nimbostratus model is generally less than that for the haze C model. This is because a greater radiation flux reaches the lower surface for a given τ value for the nimbostratus model with its strong forward scattering than for the haze C model.

The polarization curves for $\mu_0 = -0.1$ are given in Figs. 16–19. The photons near the plane of incidence have an appreciable polarization only when $A = 0$ and they are near the nadir. When $\tau = 0.1$ and ϕ is near 90°, the polarization is negative and its value is between -0.24 and -0.43 for all μ values when $A = 0$. The polarization decreases rapidly to zero when A increases from zero. When $\tau = 1$, the polarization values are generally smaller than those for $\tau = 0.1$ when $A = 0$. On the other hand, they are in general larger for $\tau = 1$ than for $\tau = 0.1$ for nonzero values of A as the unpolarized reflected radiation is polarized by collisions on its way back up through the thicker atmosphere. In some cases, such as $A = 0$ and $60° \leq \phi < 90°$, there were relatively few photons scattered into this range and so the statistical fluctuations in the result are greater than for the other curves.

The neutral points have been indicated by arrows on the figures. The neutral points for the haze C model are at approximately $\mu = 0.3$ and 0.4 when $\tau = 0.1$ and are at $\mu = 0.6$ and 0.4 when $\tau = 1$ on the side of the solar and antisolar horizons, respectively. Because of its more complicated scattering matrix, the nimbostratus model has four neutral points that are at $\mu = 0.2$ on the side near the solar horizon, at $\mu = 1$, and at $\mu = 0.5$ and 0.1 on the side near the antisolar horizon.

VII. Polarization of Transmitted Light

The polarization of the transmitted light for $\mu_0 = -1$ is shown in Fig. 20. We have again shown for comparison the polarization calculated from the scattering matrix for single scattering only. The Monte Carlo results for $\tau = 0.1$ again agree well with the single scattering results when these are averaged over the same μ intervals, except near the horizon where they are lower because of multiple scattering. The polarizations are both positive and negative for the nimbostratus model, but only positive for the haze C model. As A increases, the polarization of the transmitted light decreases, but much less rapidly than the polarization

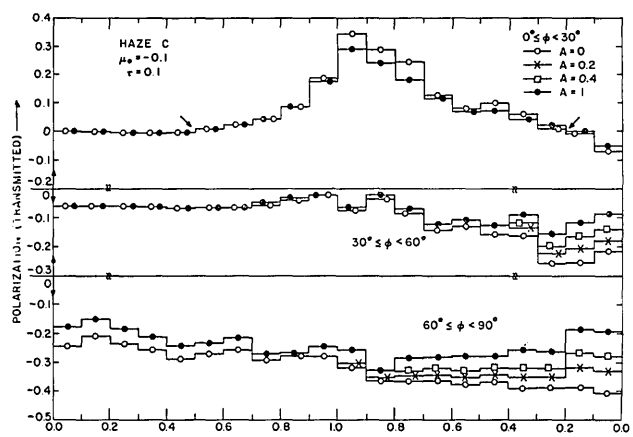

Fig. 21. Polarization of transmitted radiation as a function of μ. Curves are shown for the haze C model, $\mu_0 = -0.1$, $\tau = 0.1$, and $A = 0$, 0.2, 0.4, and 1. The results have been averaged over ϕ from 0° to 30° on both sides of the incident plane for the top set of curves; from 30° to 60° for the middle set of curves; and from 60° to 90° for the bottom set of curves.

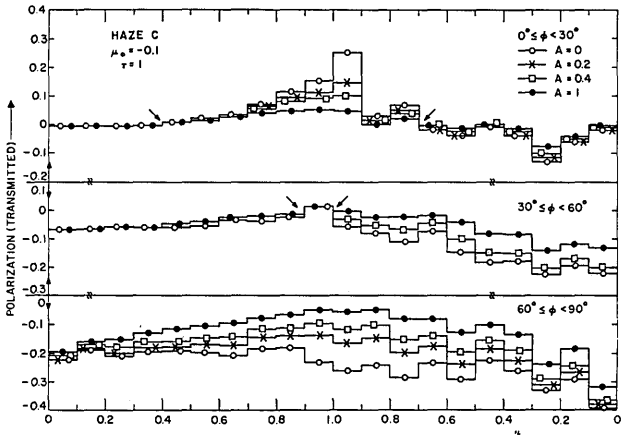

Fig. 22. Polarization of transmitted radiation as a function of μ. Same as Fig. 21 except $\tau = 1$.

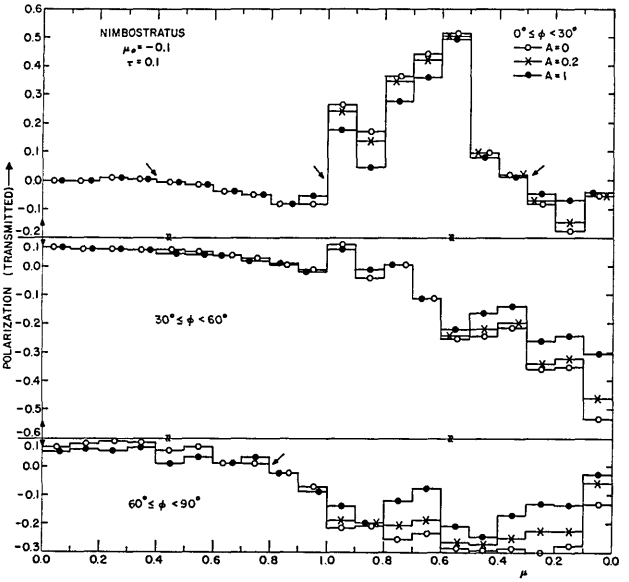

Fig. 23. Polarization of transmitted radiation as a function of μ. Same as Fig. 21 except for nimbostratus model.

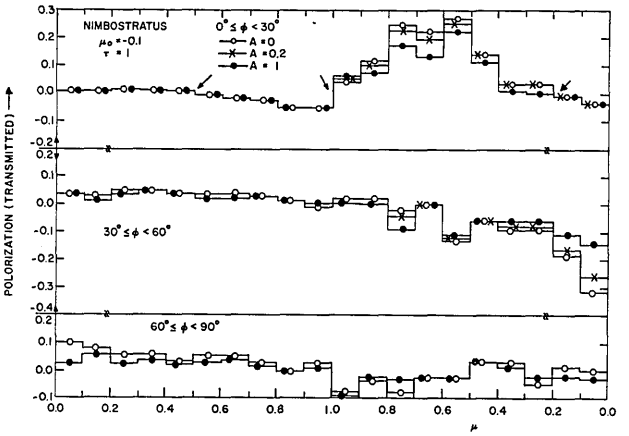

Fig. 24. Polarization of transmitted radiation as a function of μ. Same as Fig. 22 except for nimbostratus model.

of the reflected light. This is because the light reflected from the lower surface must be scattered at least once into a downward direction in order to contribute to the transmitted light; it is partially polarized by such a scattering event. Even when $A = 1$, the polarization is of the order of 0.1 over much of the range in μ for the haze C model and $\tau = 0.1$. The polarization is virtually zero in all cases near the direction of the incident beam. Except near the horizon, the polarization of the transmitted beam tends to decrease for all values of A as the optical thickness increases.

The polarization for $\mu_0 = -0.1$ is shown in Figs. 21–24. When ϕ is near 0°, the polarization is positive and has a maximum near the zenith. For larger values of ϕ, the polarization is either negative or has a small positive value. The magnitude of the polarization tends to decrease in all cases as the optical thickness increases, except possibly near the horizon. A comparison of the curves for $\mu_0 = -1$ and $\mu_0 = -0.1$ shows that the maximum polarization values tend to occur in a region approximately 90° from the direction of the incident beam. However, interesting differences show up between the models. For the haze C model, the maximum polarization occurs for ϕ near 0° in the μ interval from 1 to 0.9 in the direction of the antisolar horizon. On the other hand, for the nimbostratus model, the polarization is large for μ between 1 and 0.5 and reaches a maximum in the μ interval from 0.6 to 0.5 in the direction of the antisolar horizon. This is caused by the relatively large difference between the M_1 and M_2 components of the scattering matrix for the nimbostratus model and for scattering angles somewhat greater than 90°.

The neutral points have been indicated by arrows on the polarization curves. The nimbostratus model has an extra neutral point near the zenith since it has a region where the polarization is slightly negative from $\mu = 0.4$ to 1 in the direction of the solar horizon.

This work was supported by the Air Force Cambridge Research Laboratories Office of Aerospace Research, and by the National Aeronautics and Space Administration.

References

1. G. N. Plass and G. W. Kattawar, Appl. Opt. **7**, 415 (1968).
2. G. W. Kattawar and G. N. Plass, Appl. Opt. **7**, 361, 699, 869 (1968).
3. G. W. Kattawar and G. N. Plass, Appl. Opt. **6**, 1377 (1967).
4. S. Chandrasekhar, *Radiative Transfer* (Dover Publications, Inc., New York, 1960).
5. K. L. Coulson, J. V. Dave, and Z. Sekera, *Tables Related to Radiation Emerging from a Planetary Atmosphere with Rayleigh Scattering* (University of California Press, Berkeley, 1960).
6. H. C. Van de Hulst, *Light Scattering by Small Particles* (John Wiley & Sons, Inc., 1957).
7. S. O. Kastner, J. Quant. Spectrosc. Rad. Transfer **6**, 317 (1966).
8. D. Deirmendjian, Appl. Opt. **3**, 187 (1964).

The Optical Society of America

Officers of the Society

President	A. F. TURNER, Bausch & Lomb, Incorporated, Rochester, N.Y. 14602
President-Elect	KARL G. KESSLER, National Bureau of Standards, Washington, D.C. 20234
Past President	JOHN A. SANDERSON, OSA, 2100 Pennsylvania Avenue N. W., Washington, D.C. 20037
Executive Secretary	MARY E. WARGA, OSA, 2100 Pennsylvania Avenue N. W., Washington, D.C. 20037
Treasurer	ARCHIE I. MAHAN, Applied Physics Laboratory, 8621 Georgia Avenue, Silver Spring, Md. 20910
Editor of the Journal of the Optical Society of America	DAVID L. MACADAM, 68 Hammond Street, Rochester, N.Y. 14615
Editor of Applied Optics Research and Education	JOHN N. HOWARD, AFCRL, Bedford, Mass. 01730
Officer	JOHN A. SANDERSON, OSA, 2100 Pennsylvania Avenue N. W., Washington, D.C. 20037

Directors-at-Large

* *Term expires December 31 of the indicated year*

ROBERT P. MADDEN (68) * National Bureau of Standards, Washington, D.C. 20234
ARTHUR L. SCHAWLOW (68) * Department of Physics, Stanford University, Stanford, Calif.
RODERIC M. SCOTT (68) * Perkin-Elmer Corporation, Norwalk, Conn. 06852
KENNETH M. BAIRD (69) * National Research Council, Ottawa 2, Ont.
R. M. BOYNTON (69) * Center for Visual Science, University of Rochester, Rochester, N.Y. 14627
SUMNER P. DAVIS (69) * Department of Physics, University of California, Berkeley, Calif. 94720
B. H. BILLINGS (70) * Aerospace Corporation, El Segundo, Calif. 90245
D. R. HERRIOTT (70) * Bell Telephone Laboratories, Incorporated, Murray Hill, N. J. 07971
T. K. MCCUBBIN, JR. (70) * Physics Department, Pennsylvania State University, University Park, Pa. 16802

Local Sections

Rochester
R. J. MELTZER *President*
G. C. HIGGINS *President-Elect*
R. D. FRICKE *Secretary*
Eastman Kodak Company
343 State Street
Rochester, N.Y. 14650
C. P. SPOELHOF *Treasurer*

New England
ROBERT R. SHANNON *President*
H. E. TORBERG *Vice-President*
J. B. HOUSTON *Secretary*
Diffraction Limited, Inc.
Middlesex, Turnpike
Bedford, Mass. 02173
W. VAUGHAN *Treasurer*

Delaware Valley
H. M. FITZGERALD *President*
T. D. ROBERTS *President-Elect*
JOHN W. LANG *Secretary*
Lenox Instrument Company
111 East Luray St.
Philadelphia, Pa. 19120
M. J. OULTON *Treasurer*

National Capital
A. M. BASS *President*
C. V. MUFFOLETTO *First Vice-President*
TERRENCE L. PORTER *Secretary*
Division of Graduate Education in Science
National Science Foundation
Washington, D.C. 20550
ROBERT BRUENING *Treasurer*

Tucson
ROBERT H. NOBLE *Chairman*
P. N. SLATER *Chairman-Elect*
MICHAEL P. WIRICK *Secretary*
2122 N. Marion Blvd.
Tucson, Ariz. 85706
J. H. RICHARDSON *Treasurer*

Texas
W. E. FLYNT *President*
H. V. KENNEDY *President-Elect*
T. A. FOX *Secretary*
P. O. Box 20360
Dallas, Tex. 75220
R. J. LYSIAK *Treasurer*

Chicago
R. MOERSCH *President*
R. LEPMAN *President-Elect*
RONALD L. OHLHABER *Secretary*
IIT Research Institute
10 West 35th St.
Chicago, Ill. 60616
FRANK GLAB *Treasurer*

Greater New York
B. SHERMAN *President*
G. M. SAEPOFF *First Vice-President*
H. JUDIN *Secretary*
Areoptix Technology
P. O. Box 772
Melville, N.Y. 11746
H. B. HALLOCK *Treasurer*

Southwestern Connecticut
PAUL F. FORMAN *President*
FRANK WONG *Vice-President*
WILLIAM M. KEEFFE *Secretary*
GT&T Laboratories,
Bayside, N.Y. 11360
C. KEITH VANDERVELDEN *Treasurer*

Pittsburgh
D. M. CRAIG *President*
N. J. TRYBULA *President-Elect*
JOHN UNERTL, JR. *Secretary*
3551 East St.
Pittsburgh, Pa. 15214
R. WALTERS *Treasurer*

Southern California
J. GARDNER *President*
I. S. SANDBACK *Vice-President*
D. S. NICHOLSON *Secretary*
Aerospace Corporation
P. O. Box 95085
Los Angeles, Calif. 90045
WILFRED J. HANSEN *Treasurer*

Northern California
J. W. GOODMAN *President*
R. HASSUN *Vice-President*
B. RUFF *Secretary-Treasurer*
Spectra-Physics, Inc.
1255 Terra Bella Ave.
Mountain View, Calif. 94040

San Diego
JOHN H. BRYANT *President*
B. J. MCGLAMERY *Vice-President*
R. A. TURNER *Secretary*
U. S. Navy Electronics Laboratory
Code 3320
San Diego, Calif. 92152
R. A. ACKLEY *Treasurer*

Detroit
F. H. TOTMAN *Chairman*
R. B. FURLONG *Chairman-Elect*
JOHN A. MCLEAN *Secretary*
Chemistry Department
University of Detroit
SAMUEL COHEN *Treasurer*

Ann Arbor
R. BLYTHE *President*
G. D. COCHRAN *President-Elect*
M. BENDER *Secretary*
1617 West Stadium
Ann Arbor, Mich. 48103
J. M. VANDENBELT *Treasurer*
4001 West McNichols Road
Detroit, Michigan 48221

The Optical Society of America was organized in 1916 "to increase and diffuse the knowledge of optics in all its branches, pure and applied, to promote the mutual interests of investigators of optical problems, of designers, manufacturers and users of optical instruments, and apparatus of all kinds and to encourage cooperation among them". The Society invites to membership all who are interested in any branch of optics, either in research, in instruction, in optical or illuminating engineering, in the manufacture and distribution of optical goods of all kinds, or in physiological and medical optics. Further information may be obtained from the Executive Secretary of the Society.